

An Experimental and Computational Study of Sulfur-Modified Nucleophilicity in a Dianionic NiN₂S₂ Complex

Kayla N. Green,[‡] Scott M. Brothers,[‡] Roxanne M. Jenkins,[‡] Cody E. Carson,[‡] Craig A. Grapperhaus,[†] and Marcetta Y. Darensbourg*[‡]

Department of Chemistry, Texas A&M University, College Station, Texas 77845, and Department of Chemistry, University of Louisville, Louisville, Kentucky 40292

Received May 7, 2007

The dianionic NiN₂S₂ complex, Ni(ema)²⁻, ema = *N,N'*-ethylenebis-2-mercaptoacetamide, known as a reasonable model of the tripeptide complex Ni(CGCG)²⁻ (C = cysteine; G = glycine) with respect to the two carboxamido nitrogens and *cis*-dithiolates in a (N₂S₂)⁴⁻ ligand scaffold as found in acetyl CoA synthase, has been explored for S-based reactivity toward oxygenation and alkylation. The isolation and structural characterization of a sulfinato species, [Et₄N]₂[Ni(ema)·O₂], prepared through a unique direct reaction of molecular O₂ with crystalline [Et₄N]₂[Ni(ema)] is described. Reaction of [Et₄N]₂[Ni(ema)] with Br(CH₂)₃Br yields a neutral N₂S₂ macrocyclic complex shown by DFT computations and electrostatic-potential mapping to be opposite in electron distribution from the neutral NiN₂S₂ complexes in which the anionic charge is localized on sulfur.

Introduction

The discovery of (N₂S₂)⁴⁻ donor sites in biology based on cysteine-*X*-cysteine tripeptide motifs has prompted the examination of small molecule models that build on a well-known literature that is based on (N₂S₂)²⁻ ligands, which evolved over several decades.^{1,2} The chemistry of metallo-proteins such as acetyl CoA synthase (ACS) and nitrile hydratase (NHase) is particularly inviting in that post-translational modification is a controlling factor in enzyme activity, and such S-based reactivity can be reproduced in synthetic analogues.^{3–7}

Shown in Scheme 1 are the results of prior reactivity studies of Holm's [Ni(N₂S₂)]²⁻ complex, [Ni(ema)]²⁻, (Ni(II), ema = *N,N'*-ethylenebis-2-mercaptoacetamide), a minimal biomimetic of the Cys-Gly-Cys donor environment of the distal nickel site in ACS, containing as does ACS, two *cis*-dithiolato S donors and two carboxamido N donors.^{3,8} The sulfurs are readily alkylated with MeI and when exposed to metal sources, unique polynuclear complexes in which exogenous metals are captured by the sulfurs are obtained.^{9–13} The tungsten carbonyl derivative at the 6 o'clock position in Scheme 1 was used to establish that the donor ability of Ni(ema)²⁻ as a metallodithiolate ligand is superior to that of neutral NiN₂S₂ complexes.¹³ Nevertheless, the reactivity of Ni(ema)²⁻ largely mirrors that of neutral NiN₂S₂ complexes, emphasizing the nucleophilicity of *cis*-dithiolates, regardless of the charge on the complex.^{14–22}

* To whom correspondence should be addressed. E-mail: marcetta@mail.chem.tamu.edu. Tel.: 979 845 2981.

[†] University of Louisville.

[‡] Texas A&M University.

(1) Bouwman, E.; Reedijk, J. *Coord. Chem. Rev.* **2005**, *249*, 1555–1581 and references therein.

(2) Jicha, D. C.; Busch, D. H. *Inorg. Chem.* **1962**, *1*, 872–877.

(3) (a) Darnault, C.; Volbeda, A.; Kim, E. J.; Legrand, P.; Vernède, X.; Lindahl, P. A.; Fontecilla-Camps, J. C. *Nat. Struct. Biol.* **2003**, *10*, 271–279. (b) Doukov, T. I.; Iverson, T. M.; Seravalli, J.; Ragsdale, S. W.; Drennan, C. L. *Science* **2002**, *298*, 567–572.

(4) Nagashima, S.; Nakasako, M.; Dohmae, N.; Tsujimura, M.; Takio, K.; Odaka, M.; Yohda, M.; Kamiya, N.; Endo, I. *Nat. Struct. Biol.* **1998**, *5*, 347–351.

(5) Golden, M. L.; Rampersad, M. V.; Reibenspies, J. H.; Darensbourg, M. Y. *Chem. Comm.* **2003**, 1824–1825.

(6) Kitagawa, T.; Dey, A.; Lugo-Mas, P.; Benedict, J. B.; Kaminsky, W.; Solomon, E.; Kovacs, J. A. *J. Am. Chem. Soc.* **2006**, *128*, 14448–14449.

(7) Harrop, T. C.; Mascharak, P. K. *Coord. Chem. Rev.* **2005**, *249*, 3007–3024.

(8) Krüger, H.-J.; Peng, G.; Holm, R. H. *Inorg. Chem.* **1991**, *30*, 734–742.

(9) Duff, S. E.; Barclay, J. E.; Davies, S. C.; Evans, D. J. *Inorg. Chem. Commun.* **2005**, *8*, 170–173.

(10) Duff, S. E.; Barclay, J. E.; Davies, S. C.; Hitchcock, P. B.; Evans, D. J. *Eur. J. Inorg. Chem.* **2005**, 4527–4532.

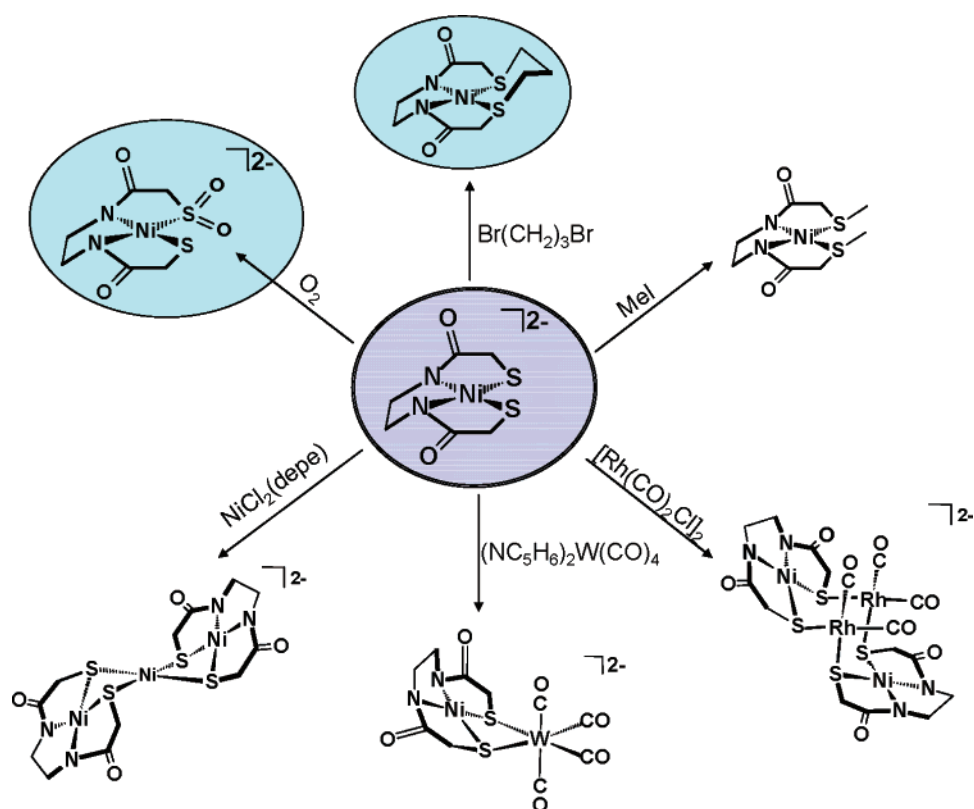
(11) Hatlevik, Ø.; Blanksma, M. C.; Mathrubootham, V.; Arif, A. M.; Hegg, E. L. *J. Biol. Inorg. Chem.* **2004**, *9*, 238–246.

(12) Jeffery, S. P.; Green, K. N.; Rampersad, M. V.; Reibenspies, J. H.; Darensbourg, M. Y. *Dalton Trans.* **2006**, *35*, 4244–4252.

(13) Green, K. N.; Jeffery, S. P.; Reibenspies, J. H.; Darensbourg, M. Y. *J. Am. Chem. Soc.* **2006**, *128*, 6493–6498.

(14) Osterloh, F.; Saak, W.; Pohl, S. J. *Am. Chem. Soc.* **1997**, *119*, 5648–5656.

Scheme 1



A recent addition to the N_2S_2 family of metalloproteins is nickel superoxide dismutase (NiSOD) which contains an N_2 -SS' trianionic site involving a His-Cys terminus dipeptide with a second cysteine three residues away.^{23–26} The interest in this active site from the view of S-based reactivity in NiN_2S_2 complexes is that it does not occur!²⁶ That is, the SOD reaction produces oxygen and peroxide in the dismu-

tation of O_2^- while avoiding S oxygenation or S oxidation.²⁶ Furthermore, a popular and reasonable mechanism proposes a Ni^{III} atom to account for the first oxidation in the ping-pong catalytic cycle.²⁴ Current computational and biomimetic investigations into the mechanism have assumed inner-sphere reactivity and have focused on the role of first coordination sphere effects in promoting Ni-based oxidative chemistry.^{26,27} For example, the influence of anionic carboxyamido nitrogens as contrasted with neutral amine donors in N_2S_2 dithiolato complexes of Ni^{II} was explored by Grapperhaus, Kozłowski, and Mullins by density functional theory (DFT), concluding that as the amine donors are sequentially replaced by anionic carboxyamido nitrogens, electron density is delocalized onto both the nickel and the sulfur atoms.²⁹ Brunold and Maroney and co-workers have suggested that the presence of even one carboxyamido nitrogen will direct redox or oxidative activity to the nickel rather than to the sulfur atom.²⁶ Nevertheless, the potential for second coordination sphere effects is obvious from the protein crystal structure, and mechanisms for sulfur protection include hydrogen bonding as well as steric interactions.^{24,29}

In view of the clear-cut connections between the synthetic and the Cys-X-Cys biological N_2S_2 ligand sets, of the likelihood that such ligand sets will be found in other biological settings, and of the great potential for S-based modification of such sites, we have endeavored to further

- (15) Linck, R. C.; Spahn, C. W.; Rauchfuss, T. B.; Wilson, S. R. *J. Am. Chem. Soc.* **2003**, *125*, 8700–8701.
- (16) Perra, A.; Davies, E. S.; Hyde, J. R.; Wang, Q.; McMaster, J.; Schröder, M. *Chem. Comm.* **2006**, 1103–1105.
- (17) Farmer, P. J.; Verpeaux, J. N.; Amatore, C. J.; Darenbourg, M. Y.; Musie, G. *J. Am. Chem. Soc.* **1994**, *116*, 9355–9356.
- (18) Kaasjager, V. E.; Bouwman, E.; Gorter, S.; Reedijk, J.; Grapperhaus, C. A.; Reibenspies, J. H.; Smee, J. J.; Darenbourg, M. Y.; Derecskei-Kovacs, A.; Thomson, L. M. *Inorg. Chem.* **2002**, *41*, 1837–1844 and references therein.
- (19) Buonomo, R. M.; Font, I.; Maguire, M. J.; Reibenspies, J. H.; Tuntulani, T.; Darenbourg, M. Y. *J. Am. Chem. Soc.* **1995**, *117*, 963–973.
- (20) Mirza, S. A.; Pressler, M. A.; Kumar, M.; Day, R. O.; Maroney, M. J. *Inorg. Chem.*, **1993**, *32*, 977–987.
- (21) Schrauzer, G. N.; Zhang, C.; Chadha, R. *Inorg. Chem.* **1990**, *29*, 4104–4107.
- (22) (a) Musie, G.; Reibenspies, J. H.; Darenbourg, M. Y. *Inorg. Chem.* **1998**, *37*, 302–310. (b) Smee, J. J.; Miller, M. L.; Grapperhaus, C. A.; Reibenspies, J. H.; Darenbourg, M. *Inorg. Chem.* **2001**, *40*, 3601–3605. (c) Smee, J. J.; Goodman, D. C.; Reibenspies, J. H.; Darenbourg, M. Y. *Eur. J. Inorg. Chem.* **1999**, 539–546. (d) Hsiao, Y.-M.; Chojnacki, S. S.; Hinton, P.; Reibenspies, J. H.; Darenbourg, M. Y. *Organometallics* **1993**, *12*, 870–875.
- (23) Choudhury, S. B.; Davidson, G.; Yim, Y.-I.; Bose, K.; Sharma, M. L.; Kang, S.-O.; Cabelli, D. E.; Maroney, M. J. *Biochemistry*, **1999**, *38*, 3744–3752.
- (24) Barondeau, D. P.; Kassmann, C. J.; Bruns, C. K.; Tainer, J. A.; Getzoff, E. D. *Biochemistry* **2004**, *43*, 8038–8047.
- (25) Wuerges, J.; Lee, J.-W.; Yim, Y.-I.; Yim, H.-S.; Kang, S.-O.; Carugo, K. D. *Proc. Natl. Acad. Sci. U.S.A.* **2004**, *101*, 8569–8574.
- (26) (a) Fiedler, A. T.; Bryngelson, P. A.; Maroney, M. J.; Brunold, T. C. *J. Am. Chem. Soc.* **2005**, *127*, 5449–5462.

- (27) Fiedler, A. T.; Brunold, T. C. *Inorg. Chem.* [Online early access]. DOI: 10.1021/ic061237k. Published Online: Feb 17, 2007.
- (28) (a) Shearer, J.; Zhao, N. *Inorg. Chem.* **2006**, *45*, 9637–9639. (b) Shearer, J.; Long, L. M. *Inorg. Chem.* **2006**, *45*, 2358–2360.
- (29) Mullins, C. S.; Grapperhaus, C. A.; Kozłowski, P. M. *J. Biol. Inorg. Chem.* **2006**, *11*, 617–625.

develop the reactivity wheel of Scheme 1 by studies of two additional S-based nucleophilic reactions of $\text{Ni}(\text{ema})^{2-}$. While the reaction of $\text{Ni}(\text{ema})^{2-}$ with O_2 had previously been reported by Hegg, et al.,¹¹ the level of O_2 incorporation into nickel dithiolates can be complicated (yielding metallo sulfinato, sulfenato, and sulfonato species), and an unambiguous characterization of the product was needed.^{17–21} The work herein reports the synthesis, characterization, and molecular structures of the dianionic sulfinate $[\text{Et}_4\text{N}]_2[\text{Ni}(\text{ema})\cdot\text{O}_2]$ and the neutral macrocyclic $\text{Ni}(\text{ema})\cdot(\text{CH}_2)_3$, derivatives of $[\text{Et}_4\text{N}]_2[\text{Ni}(\text{ema})]$. The physical properties of these $\text{Ni}(\text{ema})^{2-}$ derivatives as well as DFT calculations, natural bond orbital (NBO), and electrostatic potential (EP) analyses are contrasted within the series of $\text{Ni}(\text{ema})^{2-}$ derivatives and with certain neutral analogues.

Results and Discussion

Synthesis and Molecular Structures of Ni(II) *N,N'*-Ethylenebis(2-propylmercapto-acetamide) ($\text{Ni}(\text{ema})\cdot(\text{CH}_2)_3$) and [Tetraethylammonium][Ni(II) *N,N'*-Ethylene(*N*-mercaptoacetamide)(*N'*-sulfinatoacetamide)] ($[\text{Et}_4\text{N}]_2[\text{Ni}(\text{ema})\cdot\text{O}_2]$). On the addition of 1,3-dibromopropane to an acetonitrile solution of $[\text{Et}_4\text{N}]_2[\text{Ni}(\text{ema})]$, a red crystalline, air-stable solid of $\text{Ni}(\text{ema})\cdot(\text{CH}_2)_3$ is obtained in good yield. The $\text{Ni}(\text{ema})\cdot(\text{CH}_2)_3$ compound is insoluble in hydrocarbons, acetonitrile, dichloromethane, and tetrahydrofuran but remains soluble in methanol, DMF, and water, as does the $[\text{Et}_4\text{N}]_2[\text{Ni}(\text{ema})]$ precursor. The synthesis of $[\text{Et}_4\text{N}]_2[\text{Ni}(\text{ema})\cdot\text{O}_2]$ was accomplished via two routes. The higher yielding route results from placing dark-red $\text{Ni}(\text{ema})^{2-}$ crystals under ether and exposing the heterogeneous mixture to small quantities of air. The crystals develop into a lighter, bright-red color after 4–6 h as dioxygen diffuses into them. Alternatively, an acetonitrile solution of $[\text{Et}_4\text{N}]_2[\text{Ni}(\text{ema})]$ was slightly pressurized with $\text{O}_2(\text{g})$ and stirred for 30 min. The solution color perceptibly lightened, and the reaction was monitored for completeness using UV–vis and infrared spectroscopies.

Thermal ellipsoid plots of the square-planar $\text{Ni}(\text{ema})\cdot(\text{CH}_2)_3$ and $\text{Ni}(\text{ema})\cdot\text{O}_2^{2-}$ species as well as crystallographic data and full structural reports for $\text{Ni}(\text{ema})\cdot(\text{CH}_2)_3$ and $[\text{Et}_4\text{N}]_2[\text{Ni}(\text{ema})\cdot\text{O}_2]$ are given in the Supporting Information. The ball-and-stick drawings of Figure 1 compare metric features of $[\text{Et}_4\text{N}]_2[\text{Ni}(\text{ema})]$,⁸ $[\text{Et}_4\text{N}]_2[\text{Ni}(\text{ema})\cdot\text{O}_2]$, $\text{Ni}(\text{ema})\cdot(\text{Me})_2$,¹¹ and $\text{Ni}(\text{ema})\cdot(\text{CH}_2)_3$. Parameters of interest include a slight restriction of the S–Ni–S angle in the $\text{Ni}(\text{ema})\cdot(\text{CH}_2)_3$ macrocycle complex relative to its open-chain analogue, $\text{Ni}(\text{ema})\cdot(\text{Me})_2$, as well as $\text{Ni}(\text{ema})^{2-}$ and $\text{Ni}(\text{ema})\cdot\text{O}_2^{2-}$. This restriction is compensated by the increase of the N–Ni–N and N–Ni–S angles.

Sulfoxygenation in the $[\text{Et}_4\text{N}]_2[\text{Ni}(\text{ema})\cdot\text{O}_2]$ species results in a decreased Ni–S_{sulfinate} bond distance (2.152(2) Å), maintaining the Ni–S_{thiolate} distance (2.175(2) Å), statistically the same as that in $[\text{Et}_4\text{N}]_2[\text{Ni}(\text{ema})]$.⁸ The contracted Ni–S_{sulfinate} bond relative to the Ni–S_{thiolate} bond distances is observed in a number of sulfinate derivatives.^{17–21} The S=O bond lengths, 1.444(6) and 1.436(6) Å, are slightly shorter than those observed for neutral S oxygenates of NiN_2S_2 , which average 1.46 Å in length. Relative to $\text{Ni}(\text{ema})^{2-}$, the

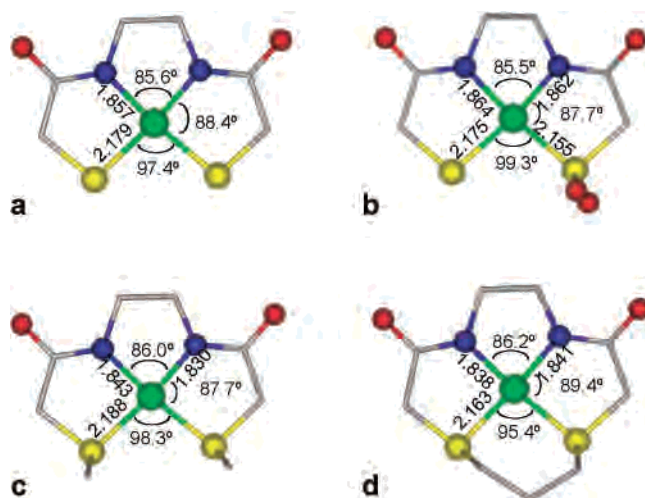
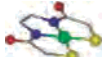
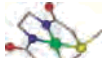
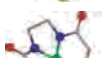



Figure 1. Structures of (a) $\text{Ni}(\text{ema})^{2-}$,⁸ (b) $[\text{Et}_4\text{N}]_2[\text{Ni}(\text{ema})\cdot\text{O}_2]$, (c) $\text{Ni}(\text{ema})\cdot(\text{Me})_2$,¹¹ and (d) $\text{Ni}(\text{ema})\cdot(\text{CH}_2)_3$ with selected bond distances (Å) and angles (deg).

Table 1. Summary of Electronic Absorption Spectra for $\text{Ni}(\text{ema})^{2-}$ (EtOH),⁸ $\text{Ni}(\text{ema})\cdot(\text{Me})_2$ (CH_3CN),¹¹ $\text{Ni}(\text{ema})\cdot(\text{CH}_2)_3$ (MeOH), and $\text{Ni}(\text{ema})\cdot\text{O}_2^{2-}$ (MeOH)

	UV–vis λ_{max} (nm) (ϵ , $\text{M}^{-1}\text{cm}^{-1}$)		
	261 (22 500)		437 (405) 552 (79)
	241 (18 200)	300 (sh, 3370)	416 (360) 490 (130)
	204 (20 200)	242 (1547)	396 (35) 476 (30)
	250 (13 841)	297 (469)	413 (35)

Ni–S_{thioether} distances are slightly elongated in the open-chain dithioether $\text{Ni}(\text{ema})\cdot(\text{Me})_2$, while in the macrocycle $\text{Ni}(\text{ema})\cdot(\text{CH}_2)_3$, the Ni–S distances are marginally shorter.⁸

Solution Characterizations of $\text{Ni}(\text{ema})\cdot(\text{CH}_2)_3$ and $[\text{Et}_4\text{N}]_2[\text{Ni}(\text{ema})\cdot\text{O}_2]$. The NMR spectrum of $\text{Ni}(\text{ema})\cdot(\text{CH}_2)_3$ in MeOH at 22 °C displays sharp signals including a pentet at 1.87 and a triplet at 2.72 ppm, assigned to the bridgehead methylene hydrogens and the two adjacent CH_2 , respectively, of the propane dithioether moiety. A doublet of doublets of AB pattern, at 3.645 and 3.488 ppm with $J_{\text{AB}} = 56$ Hz, is ascribed to the N-to-N $-\text{CH}_2\text{CH}_2-$ linker while the CH_2 units between the carbonyl and the thiolate sulfur are poorly defined underneath the methanol signal. Much broader resonances are seen in water as solvent. The infrared spectra of both $\text{Ni}(\text{ema})\cdot(\text{CH}_2)_3$ and $\text{Ni}(\text{ema})\cdot(\text{CH}_3)_2$ (in MeOH) display a band at 1582 cm^{-1} , which is ascribed to the C=O stretch of the carboxamido group.

The UV–vis absorption spectrum of $\text{Ni}(\text{ema})\cdot(\text{CH}_2)_3$ in methanol exhibits two d–d bands with λ_{max} at 396 and 476 nm as well as two intense ligand-to-metal charge-transfer bands at 204 and 242 nm. As shown in Table 1, the absorbances for both neutral alkylates are blue-shifted from those of the anionic parent complex, $[\text{Et}_4\text{N}]_2[\text{Ni}(\text{ema})]$, which is attributed to the overall stabilization of the bond and the

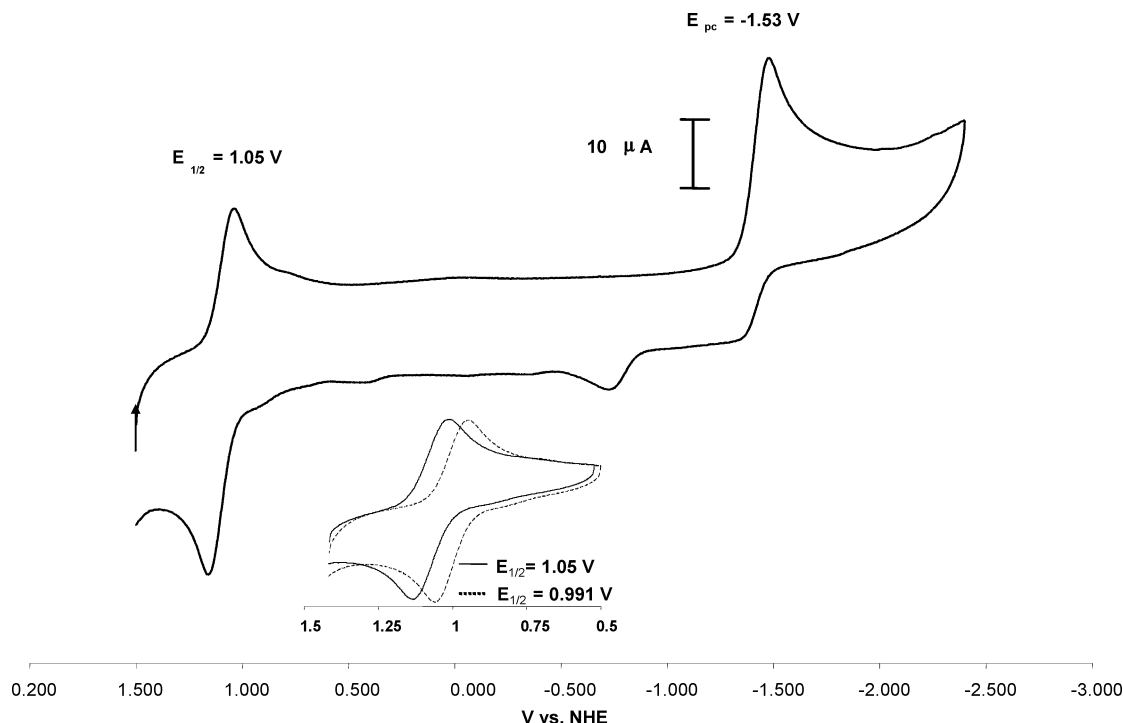


Figure 2. CV of a 3.7 mM DMF solution of Ni(ema)·(CH₂)₃ at a scan rate of 200 mV/s using a Ag/AgNO₃ reference electrode, 0.1 M [nBu₄N][BF₄] electrolyte, a glassy-carbon electrode, standardized to Fc/Fc⁺, and reported vs NHE. The inset focuses on the reversible Ni^{II/III} couple of Ni(ema)·(CH₂)₃ (solid line) and Ni(ema)·(Me)₂ (dashed line).

lone pairs on reaction with the electrophiles. A lesser blue shift of absorbances relative to those of [Et₄N]₂[Ni(ema)] is seen for the Ni(ema)·O₂²⁻ complex dissolved in methanol.

Two $\nu(\text{S}=\text{O})$ bands with a symmetric stretch at 1151 cm⁻¹ and the corresponding asymmetric stretch at 1030 cm⁻¹ are observed in the CH₃CN solution IR spectrum of Ni(ema)·O₂²⁻.¹¹ A band at 1560 cm⁻¹ (in MeOH) is assigned to the $\nu(\text{C}=\text{O})$ stretch and is the same as that of the parent Ni(ema)²⁻. The UV-vis and IR spectroscopic values correspond to those of the complex postulated by Hegg and co-workers to be the same sulfinato product produced from Ni(ema)²⁻ in an oxygenated CH₃CN solution.¹¹

The parent ion of Ni(ema)·(CH₂)₃ is observed in the positive mode of the ESI-mass spectrum as the sodium adduct at 326.98 *m/z* with the expected isotopic envelope. Crystalline material from either synthetic route that produces [Ni(ema)·O₂]²⁻ as described above has a parent isotopic bundle in the ESI-MS spectrum clustered around 239.9 *m/z*, which corresponds to [M]⁻. Additional prominent isotopic bundles containing Ni correspond to the loss of O₂ and SO₂ presumed to be induced by ionization in the ESI-MS experiment. A similar phenomenon was observed in neutral NiN₂S₂ sulfinato species.¹⁹

Electrochemical Studies. The cyclic voltammogram (CV) of Ni(ema)·(CH₂)₃ recorded in dimethylformamide (DMF) solvent is given in Figure 2 and interpreted as follows. A reversible oxidation event at +1.05 V (vs NHE) is assigned to the Ni^{II/III} couple of the Ni(ema)·(CH₂)₃ complex, and an irreversible reduction at -1.53 V is assigned to the Ni^{II/I} couple. The feature at -0.71 V is a consequence of the irreversible reduction at -1.53 V, as it is absent in scans in the anodic direction initiated at points more positive than

-1.2 V. The full-scale CV of Ni(ema)·(Me)₂, reported in Figure S3 (Supporting Information), is similar to that of Ni(ema)·(CH₂)₃ with the exception that the reductive event becomes fully reversible in the complex with a more flexible open chain. The inset in Figure 2 is an expansion of the Ni^{II/III} couple of Ni(ema)·(CH₂)₃ with that of the Ni(ema)·(Me)₂ complex overlaid.

The Ni^{II/III} couples of the dianionic Ni(ema)²⁻ and Ni(ema)·O₂²⁻ species appear as fully reversible waves at -0.160 and -0.114 V, respectively, while the Ni^{II/I} couple is shifted beyond the DMF solvent window (Figure S3, Supporting Information). While the ca. 1 V difference between the Ni^{II/III} couples of the neutral and the dianionic complexes can readily be ascribed to charge, the small difference of ca. 50 mV between the Ni^{II/III} couples of Ni(ema)·O₂²⁻ and the Ni(ema)²⁻ precursor is more subtle (Figure S4, Supporting Information). Despite S oxygenation of the thiolate sulfur and the loss of π donation, the sulfinato ligand remains a σ -donor, anionic ligand.³⁰ Apparently, there is little change in the overall electron density of the Ni^{II} atom in the two anions, and the Ni^{II/III} potential remains relatively constant. This result contrasts to electrochemical studies of analogous neutral NiN₂S₂ and NiN₂S₂·O₂ complexes with regard to differences in the Ni^{II/I} redox couple on oxygenation (the Ni^{II/III} couple being beyond the solvent window).³⁰ In these cases, the difference, +300 mV, is 6 times that observed for the difference in Ni^{II/III} couples of Ni(ema)²⁻ vs Ni(ema)·O₂²⁻. As will be discussed below, the difference between Ni(ema)²⁻ and the neutral NiN₂S₂ complexes lies in the greater covalency in the Ni-S bonds of the former

(30) Farmer, P. J.; Reibenspies, J. H.; Lindahl, P. A.; Darensbourg, M. Y. *J. Am. Chem. Soc.* **1993**, *115*, 4665-4674.

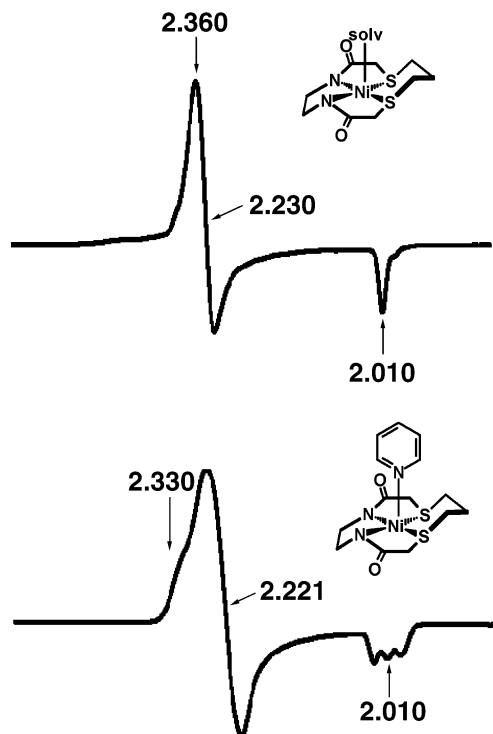


Figure 3. X-band EPR spectra obtained from an oxidized solution of Ni(ema)·(CH₂)₃ in DMF at 10 K. Simulated *g* values listed.

and in the compensatory effect of both the unmodified thiolate and the carboxyamido nitrogens, which is greater for the dianionic complexes.³¹

Electron Paramagnetic Resonance (EPR) Studies of Ni(ema)·(CH₂)₃⁺. The good reversibility of the Ni^{II/III} couple in the CV indicated the likelihood of the detection of Ni^{III} produced by bulk chemical oxidation. The EPR spectrum of the chemical oxidation product of Ni(ema)·(CH₂)₃, using cerium ammonium nitrate (CAN) in DMF solvent (Figure 3, top) displays a nearly axial EPR signal with *g*_⊥ > *g*_∥; *g* values were simulated as *g*₁ = 2.360, *g*₂ = 2.230, and *g*₃ = 2.010 (*WinEPR Simfonia* program). As *g*_{av} is significantly >2, the assignment of the product to [Ni^{III}(ema)·(CH₂)₃]⁺ with *S* = 1/2 and residence of the unpaired electron in a predominately Ni-d_{z²} orbital is reasonable. This spectrum is comparable to those reported by Holm et al., for oxidized products derived from Ni(ema)²⁻ and other diamidodithiolato NiN₂S₂ analogues.⁸ As in that work, the stabilization of the Ni^{III} oxidation state by interactions with donor molecules was probed by the oxidation of Ni(ema)·(CH₂)₃ by CAN in the presence of pyridine (pyridine/DMF, 1:4 (v/v)). The color of the reaction mixture changed from red to clear brown, as observed in the oxidation product of the complex in the absence of pyridine. The overall EPR spectral envelope is similar to that in pure DMF, with the exception of the three ¹⁴N hyperfine lines imposed on the *g*₃ = 2.01, with *a*_N = 18.5 G. The EPR spectrum thus suggests a Ni^{III} species in a *z*-axis elongated square pyramid with one nitrogen ligand in the axial coordination site. The assumption that DMF is

sufficiently coordinating to bind to Ni^{III} in the absence of pyridine would account for the identical position of the *g*₃ signal.

Computational Details of Ni(ema)²⁻, [Ni(ema)·O₂]²⁻, Ni(ema)·(CH₂)₃, and Ni(ema)·(Me)₂. DFT calculations of Ni(ema)²⁻, [Ni(ema)·O₂]²⁻, Ni(ema)·(CH₂)₃, and Ni(ema)·(Me)₂ yielded optimized structures with bond distances and angles acceptably consistent with the crystallographic experimental data; these are listed in Figure S5 (Supporting Information). DFT calculations of the Ni(ema)²⁻ complex reproduce the energies, orbital populations, and bond distances previously reported by Grapperhaus et al.²⁹ Figure 4 presents the frontier molecular orbitals of the four complexes under study. The highest-occupied molecular orbital (HOMO) of Ni(ema)²⁻ (Figure 4a) displays a clear-cut d_π-p_π antibonding orbital interaction with respect to the antisymmetric combination of the p_z orbitals of the two sulfurs (22% contribution per atom) and the d_{xz} orbital of the nickel (39% contribution). The HOMO-1, nearly degenerate with the HOMO, consists largely of the overlap of the Ni d_{yz} (44% contribution) and the symmetric combination of S p_z (14% contribution per atom). The nondegeneracy is due to the larger contributions of the amido nitrogen and carboxylate oxygen atoms, which cause slight energetic differences in the molecular orbitals. The lowest-unoccupied molecular orbital (LUMO) is an antibonding σ-orbital set comprised of 33% Ni d_{xy} character, 12% S p_{x,y} character per sulfur atom, and 4% N p_{x,y} character per nitrogen atom. The gap between the HOMO and LUMO is 4.12 eV.

As shown in Figure 4b, the electron density of the HOMO of the [Ni(ema)·O₂]²⁻ complex is localized as an antibonding orbital composed of 32% Ni d_{yz}, 45% S_{thiolate} p_z character, 4% N₍₁₎ p_z character, and 3% O₍₁₎ p_z character, where N₍₁₎ and O₍₁₎ are the amido atoms trans to S_{thiolate} and N₍₂₎ and O₍₂₎ are the amido atoms trans to S_{sulfinate}. Due to the singly modified sulfur in Ni(ema)·O₂²⁻, the near-degeneracy of the HOMO and HOMO-1 orbitals of the Ni(ema)²⁻ parent complex is broken. Nevertheless, as in Ni(ema)²⁻, the HOMO-1 still appears to be a bonding orbital orthogonal to the HOMO with considerable electron density on the Ni d_{xz}, N₍₂₎ p_z, and O₍₂₎ p_z orbitals (36, 20, and 13% contributions, respectively). The LUMO has a small percentage of electron density on the sulfinate oxygens but in other respects is largely the same as that of the Ni(ema)²⁻ parent complex. Interestingly, the HOMO-LUMO gap of this oxygenated complex is nearly identical to that in the parent complex, i.e., 4.15 eV.

In Ni(ema)·(Me)₂ and Ni(ema)·(CH₂)₃, the HOMO and the HOMO-1, shown in parts c and d of Figure 4, largely reflect the analysis described above for the *cis*-dithiolate. That is, the asymmetric combination of the N p_z orbitals (16–18% contribution per atom) engages in antibonding overlap with the Ni d_{xz} orbital (21–22% contribution), producing the HOMO, and the symmetric combination of the N p_z orbitals (10–15% contribution per atom) with Ni d_{yz} (19–20% contribution) makes up the HOMO-1. A more substantial contribution from the O p_z orbitals (5–10% contribution)

(31) Lugo-Mas, P.; Dey, A.; Xu, L.; Davin, S. D.; Benedict, J.; Kaminsky, W.; Hodgson, K. O.; Hedman, B.; Solomon, E. I.; Kovacs, J. A. *J. Am. Chem. Soc.* **2006**, *128*, 11211–11221.

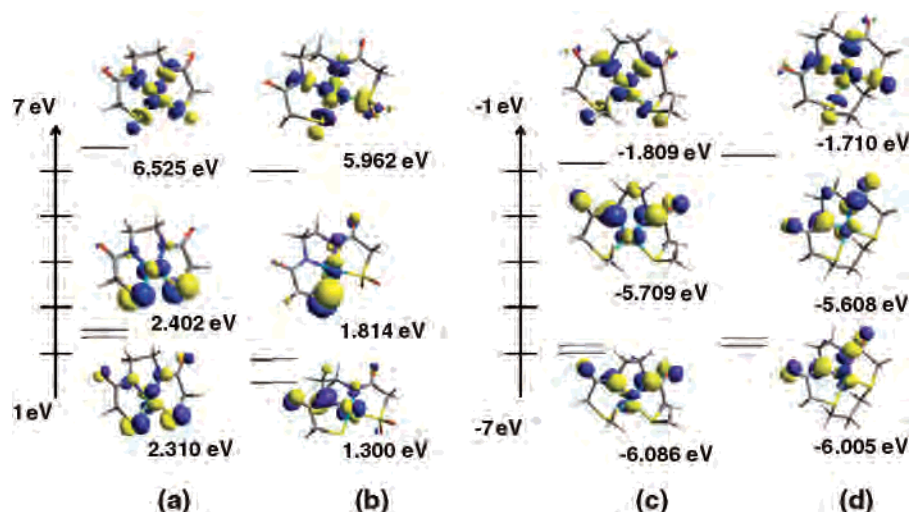


Figure 4. Frontier molecular orbitals of (a) $\text{Ni}(\text{ema})^{2-}$, (b) $[\text{Ni}(\text{ema})\cdot\text{O}_2]^{2-}$, (c) $\text{Ni}(\text{ema})\cdot(\text{CH}_3)_2$, and (d) $\text{Ni}(\text{ema})\cdot(\text{CH}_2)_3$. In each column, the orbitals descend in the order LUMO, HOMO, and HOMO-1.

relative to the parent $\text{Ni}(\text{ema})^{2-}$ complex is also observed. Again, the LUMO is in the σ framework of the square plane.

Natural Bond Orbital Analysis. Natural bond orbital (NBO) analysis is a technique derived from density functional theory as a powerful tool for clarification of the principal resonance structures of the molecule under study. Atomic charges from geometry optimization are used to determine the primary ground-state structure. Delocalization of the electrons and resonance structures of the molecule is derived from second-order effects. In the current study, this technique was employed to assign formal dative or coordinate-covalent bond character between the Ni–N and Ni–S bonds, which undergo significant change upon modification of the thiolate sulfurs. This consequently affects electron delocalization in the amido framework.

The NBO analysis of $\text{Ni}(\text{ema})^{2-}$ indicates an electronic population per covalent bond between the nickel and each sulfur atom of 1.95 electrons, with no covalency in the bond between nickel and nitrogen atoms. According to this analysis, 1.71 electrons were found on each nitrogen atom in an sp^2 hybridized orbital, with a strongly stabilized donor–acceptor interaction between this quasi-lone pair and the corresponding *trans* Ni–S* antibond, which has 0.296 electrons in the most stable resonance structure. This stabilization is further indicative of a dative bond between the nickel and the nitrogen atoms with fully covalent bonds between the nickel and the sulfur atoms. At the 6-311G-(d,p) level of theory, the second nitrogen lone pair on each nitrogen atom was not found; however, two bonds between nitrogen and the adjoining carbon atom were located with electronic populations of 1.99 and 1.78. The small electronic population of the second N–C_{amido} bond is a result of the missing lone pair on the nitrogen atom as part of the delocalized amido system. By the use of a hybrid basis set at a higher level of theory, the second nitrogen lone pair was resolved (see the Supporting Information).

The NBO analysis of the S-alkylated complexes is also consistent with the DFT computations, for a reversal of the major contributing atoms in the NiN_2S_2 core to the ground-

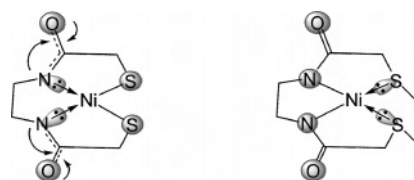


Figure 5. Principal resonance structures of $\text{Ni}(\text{ema})^{2-}$ and $\text{Ni}(\text{ema})\cdot(\text{CH}_3)_2$ as identified by NBO analysis. Dative bonds are a donation of the lone pair shown on the tail of the arrow into the corresponding *trans* Ni–X antibond (X = S, N).

state electronic structure is also found in these results. In the case of $\text{Ni}(\text{ema})\cdot(\text{CH}_2)_3$, the nickel is covalently bonded to each nitrogen with an electronic bond population of 1.93 electrons, whereas each of the sulfur atoms has a lone pair of 1.72 electrons primarily in a p orbital with a slight amount of s mixing. This dative sulfur interaction has a large energetic stabilization through delocalization of these electrons into the Ni–N* antibond (0.318 electrons). This indicates that following the alkylation of the sulfurs of $\text{Ni}(\text{ema})^{2-}$, the formal dative bonds in the NiN_2S_2 core reverse positions. Also interesting to note is that, in contrast to the parent complex $\text{Ni}(\text{ema})^{2-}$, two fully covalent bonds exist between the carbon and oxygen on the amido backbone, indicating a significant decrease in delocalization. This result is graphically displayed in Figure 5.

Electrostatic Potentials. The electrostatic potential maps of $\text{Ni}(\text{ema})^{2-}$ and the related derivatives are displayed in Figure 6. The color coding for positive potential (blue) and negative potential (red) of the atoms in each compound readily mirrors the change in electronic distribution through the series and the sites of greatest potential reactivity. It should be noted that due to the difference in electrostatic parameters between neutral and dianionic complexes, only a qualitative comparison of the surfaces is possible. The sites of greatest negative potential in the NiN_2S_2 core of $\text{Ni}(\text{ema})^{2-}$ are the lone pairs on the thiolate sulfurs, indicating that reactions at these sites with electrophiles should be facile, as has been found. Furthermore, the negative character of the amido nitrogens is on the lone pairs on the p_z orbitals; however, this negative character is a great deal less than the

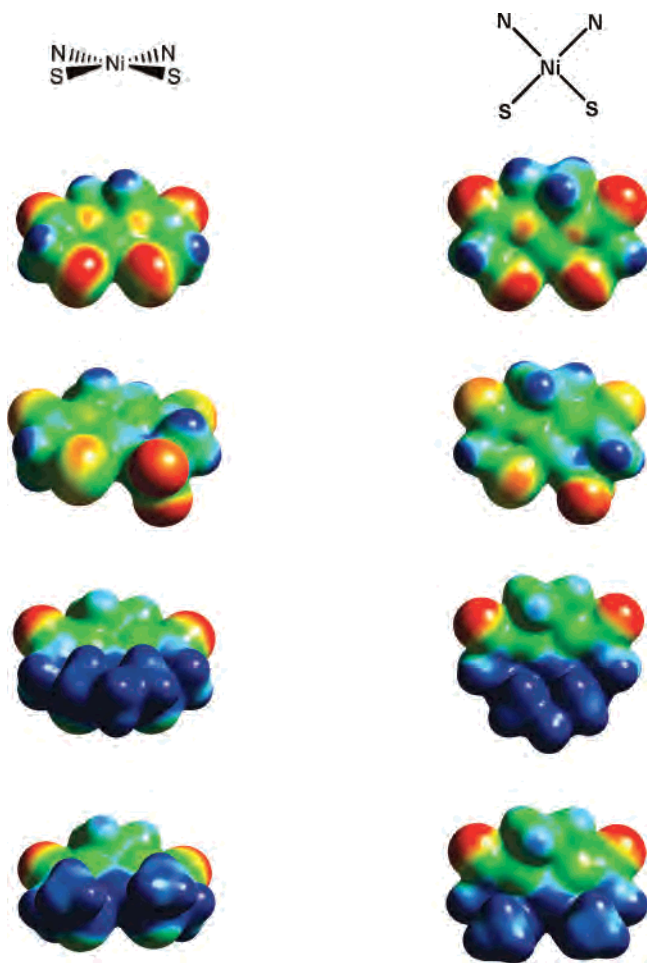


Figure 6. In order of descent: Electrostatic potentials of $\text{Ni}(\text{ema})^{2-}$, $[\text{Ni}(\text{ema})\cdot\text{O}_2]^{2-}$, $\text{Ni}(\text{ema})\cdot(\text{CH}_2)_3$, and $\text{Ni}(\text{ema})\cdot(\text{Me})_2$. The range was taken from 1.00 (the most electropositive region, dark blue) to 0.33 (the most electronegative region, bright red). Views are along the bisector of the S–Ni–S angle and from the top as noted.

corresponding thiolate sulfur character. These results correlate with the dative bond–covalent bond argument presented by the NBO analysis.

Upon oxygenation of one of the thiolate sulfurs, pronounced changes occur as follows. The electron density localized on the thiolate sulfurs in the parent $\text{Ni}(\text{ema})^{2-}$ complex shifts onto the lone pairs of oxygens on the sulfenato group. In addition, upon the incorporation of oxygen into $\text{Ni}(\text{ema})^{2-}$, electron density is withdrawn from the thiolate sulfur cis to the sulfenato sulfur, which is expected to decrease the reactivity of the thiolate sulfur with additional dioxygen or electrophiles. The electron density of the amido nitrogens is also decreased following the S oxygenation of $\text{Ni}(\text{ema})^{2-}$. This shift is consistent with computational studies by Maroney et al. on neutral NiN_2S_2 complexes.³² Interestingly, such a withdrawal of electron density from the overall NiN_2S_2 core via S oxygenation is similar to that experienced from H bonding to a single thiolate.^{29,30} Both effects serve to deactivate the remaining thiolate sulfur with significant implication for biological systems that use analogous peptidic MN_2S_2 active sites.^{29,31} Finally, the alkylation of the thiolates

in $\text{Ni}(\text{ema})^{2-}$ with electrophiles such as CH_3^+ or $(\text{CH}_2)_3^{2+}$ produces pronounced changes in the EP maps as suggested by DFT and NBO calculations. In the thioether or the macrocycle, the negativity of the thiolate sulfurs of $\text{Ni}(\text{ema})^{2-}$ is almost completely quenched, leaving behind only a slight negative character on the lone pair oriented exo to the NiN_2S_2 core. As compared with the modified sulfur atoms in $\text{Ni}(\text{ema})\cdot(\text{Me})_2$ and $\text{Ni}(\text{ema})\cdot(\text{CH}_2)_3$, the amido nitrogen atoms are the sites of greater negativity, owing to the lone pair and formal negative charge on the nitrogen. It is important to note that in the parent complex $\text{Ni}(\text{ema})^{2-}$ and all of the derivatized complexes presented herein, the use of the Mulliken or the atomic charges as the basis for the electrostatic potentials indicates little to no negative character on the nickel center.

Conclusions

The isolation of $[\text{Ni}(\text{ema})\cdot\text{O}_2]^{2-}$ and $\text{Ni}(\text{ema})\cdot(\text{CH}_2)_3$ demonstrates that thiolate S-based reactivity of the dianionic NiN_2S_2 complexes based on carboxamido nitrogen donor scaffolds is as extensive as that previously established for neutral analogues with primary and secondary amine frameworks. The $[\text{Ni}(\text{ema})\cdot\text{O}_2]^{2-}$ complex, reported earlier by Hegg, et al.¹¹ and isolated here for full characterization, is the first dianionic $\text{NiN}_2\text{S}_{\text{thiolate}}\text{S}_{\text{sulfinate}}$ derived from controlled reactivity of $\text{NiN}_2\text{S}_2^{2-}$ with O_2 to form a sulfinato complex analogous to neutral NiN_2S_2 complexes. In this study, we find that a solid-state reaction of crystalline $[\text{Et}_4\text{N}]_2[\text{Ni}(\text{ema})]$ is the most efficient mode of preparation. The unambiguous characterization of $[\text{Et}_4\text{N}]_2[\text{Ni}(\text{ema})\cdot\text{O}_2]$ via X-ray crystallography is significant in that the conventional expectation of outer-sphere oxidation producing a Ni^{III} or ligand oxidation with degradation can be avoided under the correct synthetic approach.

It is of consequence that mild conditions involving dioxygen at ambient pressures lead to S oxygenates of both neutral and dianionic NiN_2S_2 complexes. *Qualitatively, the latter are significantly more reactive.* Maroney and co-workers have noted an increased reactivity with anionic NiNS_2 systems as well.³² As stated by Shearer et al. and Grapperhaus and et al., a mixed amido/amine complex should show reactivity between the neutral NiN_2S_2 and the anionic $\text{NiN}_2\text{S}_2^{2-}$.^{28,29} This has been experimentally established by Shearer and co-workers, who demonstrated that a mixed carboxamido/amine complex is more stable in the presence of O_2 as compared with an analogous dicarboxamido species.²⁹ Nevertheless, rates of reaction with O_2 appear to be much slower, even in the dianionic complexes, than rates responsible for the turnover frequency of NiSOD (reported as $k_{\text{cat}} = 10^9 \text{ M}^{-1} \text{ s}^{-1}$ per Ni).³² This difference is a palpable answer to the lack of destruction of the enzyme active site as deleterious products arise; however, a definitive answer awaits further study.

The cyclic voltammogram of $[\text{Ni}(\text{ema})\cdot\text{O}_2]^{2-}$ shows that sulfoxy modifications of dithiolates fine-tune the $\text{Ni}^{\text{III/II}}$ redox couple of dianionic complexes. This result is of significance to enzymatic systems, which use the Cys-Ser-Cys peptide backbone as an N_2S_2 binding site, post-translationally modi-

(32) Maroney, M. J.; Choudhury, S. B.; Bryngelson, P. A.; Mirza, S. A.; Sherrod, M. J. *Inorg. Chem.* **1996**, *35*, 1073–1076.

fied by sulfoxylation, as found in cobalt and iron NHase. It has been proposed that the sulfoxylated groups of the N_2S_2 peptidic ligand are required to regulate the Lewis acidity of the metal for the conversion of metal-bound nitriles to amines.³¹

DFT studies and derived parameters from NBO and EP analyses report on the electron distribution in the dianionic NiN_2S_2 complexes and neutral derivatives derived from alkylation. Despite the formal negative charge on each N and S donor atom in $Ni(ema)^{2-}$, reactivity with electrophiles is at sulfur. Once the active lone pairs of the thiolato sulfurs are quenched by covalent bond formation with carbon or oxygen, the negative charge in the carboxamido frame becomes localized on nitrogen, creating, in the NBO analysis, covalent bond character in the N–Ni bond with the dative bond character shifting into the thioether S to Ni bond. The electrostatic-potential maps show that the polar character of the carboxyamido groups remains in the neutral derivatives as sites for H bonding, explaining the solubility characteristics in H-bonding solvents. Nevertheless, further reactivity with electrophiles is lost, yielding a class of dianionic tetradentate N_2S_2 ligands and stable, tractable neutral NiN_2S_2 complexes for the exploration of metal-based redox activity and reactivity.

Methods and Materials

General Methods. Solvents were purified according to standard procedures and were freshly distilled under N_2 prior to use or purified and degassed via a Bruker solvent system.³³ Other reagents were purchased from commercial sources and used as received unless noted. Cerium ammonium nitrate (CAN) was used as obtained from Strem Chemicals.

Syntheses of air-sensitive $Ni(II)$ complexes were performed under anaerobic conditions using distilled/degassed solvents and standard Schlenk-line techniques under an argon atmosphere. The $[Et_4N^+]_2[Ni(ema)^{2-}]$ and $Ni(ema) \cdot (Me)_2$ complexes were prepared following published procedures and used in CV analysis to be consistent with conditions used for the new complexes reported herein.^{8,11}

Physical Methods. Solution infrared spectra were recorded on a Bruker Tensor 27 FTIR spectrometer using 0.1 mm NaCl sealed cells. UV–vis spectra were recorded on a Hewlett-Packard HP8452A diode array spectrometer. Mass spectrometry (ESI-MS) was performed by the Laboratory for Biological Mass Spectrometry at Texas A&M University. Elemental analyses were performed by the Canadian Microanalytical Services, Ltd., Delta, British Columbia, Canada. Cyclic voltammograms were obtained under an Ar atmosphere at 22 °C using a BAS100W potentiostat equipped with a 3.0 mm glassy-carbon working electrode, a platinum-wire auxiliary electrode, and a $Ag/AgNO_3$ reference electrode. Measurements were performed in a DMF solution with 0.1 M $[Bu_4N][BF_4]$ as supporting electrolyte. Ferrocene was used as an internal standard, and the values reported are relative to NHE ($Fc/Fc^+ = +692$ mV in DMF vs NHE).³⁴ EPR spectra were obtained with a Bruker ESP 300 equipped with an Oxford ER910 cryostat operating at 10 K. Samples were 1 mM in analyte in DMF and frozen in

liquid N_2 prior to recording the EPR spectra at 10 K. The g values reported were as simulated using the *WinEPR Simfonia* program.³⁵

Structure Solution and Refinement. A Bruker SMART 1000 X-ray three-circle diffractometer was employed for crystal screening, unit-cell determination, and data collection. The goniometer was controlled using the *SMART* software suite, version 5.625. The X-ray radiation employed was generated from a Mo sealed X-ray tube ($K\alpha = 0.70173$ Å, with a potential of 50 kV and a current of 40 mA) and filtered with a graphite monochromator in the parallel mode (175 mm collimator with 0.5 mm pinholes). Integrated intensity information for each reflection was obtained by reduction of the data frames with the program *SAINT*, version 6.63.³⁶ The integration method employed a three-dimensional profiling algorithm, and all data were corrected for Lorentz and polarization factors, as well as for crystal-decay effects. Finally, the data was merged and scaled to produce a suitable data set. The absorption correction program *SADABS* was employed to correct the data for absorption effects.³⁷ *X-Seed* was employed for the final data presentation and structure plots.³⁸ The tetraethylammonium cation of **2** in MeCN was found to be disordered between two positions. The anions were modeled by employing local bond distance restraints and included in the final refinement. The CCDC reference nos. are 637429 and 637428.

Computations. DFT calculations, including geometry optimization and NBO analysis, were performed using a hybrid functional (the three-parameter exchange functional of Becke (B3)³⁹ and the correlation functional of Lee, Yang, and Parr (LYP)⁴⁰) (B3LYP) as implemented in *Gaussian 03*.⁴¹ For each calculation, all atoms were optimized via the use of the 6-311g(d,p) basis set. Additional NBO calculations were performed with a mixed basis set using Dunning's correlated consistent polarized valence double- ζ (cc-pVDZ) for nitrogen and sulfur atoms,⁴² D95 for hydrogen atoms,⁴³ and double- ζ + polarization (DZP) for carbon and oxygen atoms.⁴⁴ The nickel center was calculated using a contracted cc-pVTZ basis set, whereby the last shell of each type of function was removed to form a cc-pVDZ basis set. Cartesian coordinates for the starting input geometries were extracted from the crystallographic structures.

(35) *WinEPR Simfonia*, version 1.25; Bruker Analytische Messtechnik GmbH, 1996.

(36) *SAINT*, version 6.63, *Program for Reduction of Area Detector Data*; Bruker AXS, Inc.: Madison, WI.

(37) Sheldrick, G. M. *SADABS, Program for Absorption Correction of Area Detector Frames*; Bruker AXS, Inc.: Madison, WI.

(38) Barbour, L. J. *X-Seed, A Software Tool for Supramolecular Crystallography*. *J. Supramol. Chem.* **2001**, *1*, 189–191.

(39) Becke, A. D. *J. Chem. Phys.* **1993**, *98*, 5648.

(40) Lee, C.; Yang, W.; Parr, R. G. *Phys. Rev.* **1988**, *37*, 785.

(41) Frisch, M. J.; Trucks, G. W.; Schlegel, H. B.; Scuseria, G. E.; Robb, M. A.; Cheeseman, J. R.; Montgomery, J. A., Jr.; Vreven, T.; Kudin, K. N.; Burant, J. C.; Millam, J. M.; Iyengar, S. S.; Tomasi, J.; Barone, V.; Mennucci, B.; Cossi, M.; Scalmani, G.; Rega, N.; Petersson, G. A.; Nakatsuji, H.; Hada, M.; Ehara, M.; Toyota, K.; Fukuda, R.; Hasegawa, J.; Ishida, M.; Nakajima, T.; Honda, Y.; Kitao, O.; Nakai, H.; Klene, M.; Li, X.; Knox, J. E.; Hratchian, H. P.; Cross, J. B.; Bakken, V.; Adamo, C.; Jaramillo, J.; Gomperts, R.; Stratmann, R. E.; Yazyev, O.; Austin, A. J.; Cammi, R.; Pomelli, C.; Ochterski, J. W.; Ayala, P. Y.; Morokuma, K.; Voth, G. A.; Salvador, P.; Dannenberg, J. J.; Zakrzewski, V. G.; Dapprich, S.; Daniels, A. D.; Strain, M. C.; Farkas, O.; Malick, D. K.; Rabuck, A. D.; Raghavachari, K.; Foresman, J. B.; Ortiz, J. V.; Cui, Q.; Baboul, A. G.; Clifford, S.; Cioslowski, J.; Stefanov, B. B.; Liu, G.; Liashenko, A.; Piskorz, P.; Komaromi, I.; Martin, R. L.; Fox, D. J.; Keith, T.; Al-Laham, M. A.; Peng, C. Y.; Nanayakkara, A.; Challacombe, M.; Gill, P. M. W.; Johnson, B.; Chen, W.; Wong, M. W.; Gonzalez, C.; Pople, J. A., Jr. *Gaussian 03*, revision C.02; Gaussian, Inc.: Wallingford, CT, 2004.

(42) Dunning, T. H. *J. Chem. Phys.* **1989**, *98*, 1007.

(43) Dunning, T. H. *J. Chem. Phys.* **1970**, *53*, 2823.

(44) Dunning, T. H.; Hay, P. J. In *Methods of Electronic Structure Theory*; Schaefer, H. F., III, Ed.; Plenum Press, 1977; Vol. 2.

(33) Gordon, A. J.; Ford, R. A. *The Chemist's Companion*; Wiley and Sons: New York, 1972; pp 429–436.

(34) Connelly, N. G.; Geiger, W. E. *J. Am. Chem. Soc.* **1996**, *96*, 877–910.

A frequency calculation was performed alongside each geometry optimization to ensure the stability of the ground state as ascertained by the absence of imaginary frequencies. Graphical visualizations of the electron density of the individual molecular orbitals and the electrostatic potentials were first generated as cube files from *Gaussian*, and these images were implemented into and viewed by the *Cerius²* software package.⁴⁵ Optimized geometries of each of the complexes were imported into and visualized with *JIMP2*.⁴⁶ Geometric parameters were extracted from the optimized structures by use of the *GaussView* program.⁴⁷ For each complex in this text, the energies have been converted from values in hartrees to eV.

Synthesis of Ni(II) *N,N'*-Ethylenebis(2-propylmercaptoacetamide), Ni(ema)·(CH₂)₃. To a dark-red solution of Ni(ema)²⁻ (120 mg, 0.230 mmol in 30 mL CH₃CN), dibromopropane (23 μL, 0.230 mmol) was added via microsyringe. The solution developed a bright-red hue, was stirred for 20 min, and stored at -20 °C. Red, X-ray-quality blocks were obtained after 3 days: 41.6 mg (59% yield). Anal. Calcd (Found) for C₉H₁₄N₂NiO₂S₂: C 35.44 (34.83), N 4.63 (4.68), H 9.02 (9.18). Absorption spectrum (MeOH): λ_{max} (ε, M⁻¹ cm⁻¹) 204 (20,200), 242 (1,547), 396 (79), 476 (29) nm. ⁺ESI-MS: *m/z* 326.98 [M + Na]⁺, 304.5 [M + H]⁺. Decomposition point: 233 °C.

Synthesis of Ni(II) *N,N'*-Ethylene(*N*-mercaptoacetamide)(*N'*-sulfinatoacetamide), [Et₄N]₂[Ni(ema)·O₂]. (Route A) A 100 mL Schlenk flask containing a dark-red solution of Ni(ema)²⁻ (50 mg, 0.96 mmol in 20 mL CH₃CN) was backfilled with O₂(g) and stirred for 30 min. The solution was filtered through celite and layered with ether to yield bright-red X-ray-quality block crystals after 2 weeks. Yield: 16 mg (29%). (Route B) A CH₃CN solution of

Ni(ema)²⁻ (100 mg, 0.19 mmol in 20 mL CH₃CN) was layered with ether to obtain dark-red crystals of [Et₄N]₂[Ni(ema)] after 1 week.⁸ The supernatant was removed and replaced with ether, covering all crystalline material. The flask was then exposed to small quantities of air, and the resulting bright-red X-ray-quality crystals of [Et₄N]₂[Ni(ema)·O₂] were collected after 1 day. Yield: 83 mg (78%). Anal. Calcd (Found) for C₂₂H₄₈N₄NiO₄S₂: C 47.57 (47.64), N 10.09 (10.66), H 8.71 (9.43). Absorption spectrum (MeOH): λ_{max} (ε, M⁻¹ cm⁻¹) 250 (13,841), 297 (469), 413 (35) nm. ⁻ESI-MS: (*m/z*) 293.9 [M + H]⁻, 262.93 [M + H - O₂]⁻, 229.97 [M + H - SO₂]. Melting point: 157.5–159 °C. IR (CH₃-CN) ν(S=O) 1151, 1030 cm⁻¹. Oxidation of Ni(ema)·(CH₂)₃. To a 1 mg (4 × 10⁻⁶ mol) sample of Ni(ema)·(CH₂)₃ dissolved in 4 mL of DMF was added 2 mg (1 equiv) of solid CAN at 22 °C. The red solution turned to a clear brown color within 10 s; over the course of minutes, the solution turned yellow with subsequent complete bleaching. An EPR sample of the brown product was obtained by placing 200 μL of the reaction mixture into a 5 mm tube and immediately freezing in liquid N₂. With NOBF₄ as the oxidant, no reaction was observed.

Acknowledgment. We acknowledge financial support from the National Science Foundation (CHE-0616695 to M.Y.D.) with contributions from the R. A. Welch Foundation (A-0924) and the National Institutes of Health (Chemistry-Biology Interface Training Grant to K.G. and R.J., T32 GM008523). We thank the TAMU X-ray crystallography facility and Dr. J. H. Reibenspies as well as Dr. Lisa Perez and the Laboratory for Molecular Simulation at Texas A&M University. Helpful discussions with Dr. Abhishek Dey are greatly appreciated.

Supporting Information Available: Full structure (CIF) file; cyclic voltammograms; further computational details. This material is available free of charge via the Internet at <http://pubs.acs.org>.

IC700878Y

(45) *Cerius²*, version 3.0; MSI: Cambridge, U.K.

(46) Manson, J. M. B.; Webster, C. E.; Hall, M. B. *JIMP 2*, version 0.91, 1/8/07, Microsoft Windows XP; Department of Chemistry: Texas A&M University, College Station, TX; <http://www.chem.tamu.edu/jimp2/>.

(47) Dennington, R., II; Keith, T.; Millam, J.; Eppinnett, K.; Hovell, W. L.; Gilliland, R.; *GaussView*, version 3.09; Semichem, Inc.: Shawnee Mission, KS, 2003.